Advances in Differential Equations and Control Processes 2026, 33(3), 4719.
doi: https://doi.org/10.59400/adecp4719

Article

Improving the aerodynamic stability and controllability of aircraft, considering the speed of sound and maneuvering oscillations under disturbing atmospheric conditions

Toghrul Karimli[1], Aftandil Mammadov[1,*], Rauf Guliyev[1], Elnur Asadov[1], Vasif Karimli[2]

[1] Department of Avionics, Faculty of Air Transport, National Aviation Academy, Baku AZ1045, Azerbaijan; tkarimli@naa.edu.az (TK); rauf.quliyev@naa.edu.az (RG); elnur.asadov@naa.edu.az (EA)

[2] Azerbaijan Airlines, Baku AZ1000, Azerbaijan; vkarimli@azal.az

*** Corresponding authors:** Aftandil Mammadov, aftandilmammadov@naa.edu.az

CITATION

Karimli T, Mammadov A, Guliyev R, et al. Improving the aerodynamic stability and controllability of aircraft, considering the speed of sound and maneuvering oscillations under disturbing atmospheric conditions. Advances in Differential Equations and Control Processes. 2026; 33(3): 4719.
https://doi.org/10.59400/adecp4719

ARTICLE INFO

Received: 24 July 2026
Revised: 21 August 2026
Accepted: 26 August 2026
Available online: 1 September 2026

Abstract: An aircraft's aerodynamic stability and controllability in pitch, roll, and yaw are determined by its flight performance and actual flight conditions. Traditional stability augmentation systems based on gyroscopic and inertial feedback are activated only after a disturbance has been applied, so the aircraft first acquires unwanted angular deflections and kinetic energy that must subsequently be damped. This article proposes an integrated smart aerometric approach that enables early detection of atmospheric disturbances before they affect the aircraft dynamics. Its key element is an atmospheric disturbance monitoring unit based on smart aerometric sensors located on the wingtips and in the tail section. Coupled with advanced feedback structures in the pitch, roll, and yaw channels, these sensors reduce transient response time and improve stability and control in turbulent conditions. The concept is evaluated by comparative modeling in MATLAB/Simulink for classical, modern, and proposed flight control architectures, with true airspeed relative to the speed of sound (Mach number) and load factor taken as the key flight parameters. In stable flight, adaptive modification of the transfer function coefficients increases the stability margin and prevents autopilot disengagement under intense turbulence and overload; in maneuvering mode, automatic coefficient readjustment improves controllability by reducing excess stability. The results of mathematical modeling indicate that the proposed approach reduces the amplitude and duration of damped transient processes during maneuvering. An explicit adaptive gain-scheduling law, a closed-loop stability analysis, and a quantitative case study with performance indices and robustness evaluation are also presented.

Keywords: sound speed; amplitude; frequency; transient process; aerometric stability; aircraft controllability; smart probe

1. Introduction

Aircraft flight is a complex physical and engineering process in which the aircraft's structure, aerodynamic forces, flight characteristics, and environmental conditions are constantly depending on each other's performances [1]. During flight, an aircraft must have several characteristics to generate sufficient lift, overcome drag, ensure structural safety, and maintain control under various meteorological influences, such as persistent atmospheric disturbances such as turbulence, wind gusts, wake vortices, icing, and sudden changes in altitude and temperature.

Aircraft stability and controllability are not constant properties; they depend on multiple factors such as aircraft configuration, speed, altitude, air density, Mach number, load factor, and control surface effectiveness [1,2].

Traditional flight control and stability augmentation systems typically respond after an aircraft's pitch, roll, or yaw input has already occurred [2,3]. Under normal flight conditions, this feedback-based correction is generally sufficient. However, in a disturbed atmosphere, delaying the correction can increase the amplitude of oscillations and prolong the transient response, as well as reduce aircraft controllability. This study explores the possibility of improving aircraft stability and controllability by using aerometric information from smart sensors for earlier detection of airflow disturbances and adaptive correction of aircraft rotational motion along multiple axes.

It should be clearly stated that the underlying aircraft dynamics, transfer-function models, and Mach-number relations used in this study are classical and well established; the novelty of the proposed approach lies not in the mathematical formulation itself, but in the additional aerometric feedback path and the associated adaptive gain-scheduling law, which provide earlier disturbance detection than conventional gyroscopic and inertial feedback alone.

1.1. Flight performance characteristics

Flight performance is the ability of an aircraft to operate safely while maintaining speed, altitude, maneuverability, and controllability under Mach-dependent and atmospheric disturbances [1–5]. Aircraft flight is governed by the classical balance of lift, weight, thrust, and drag, and by the resulting pitching, rolling, and yawing moments generated by aerodynamic forces about the center of gravity [1–4]. These forces and moments depend on air density, airspeed, angle of attack, aircraft configuration, mass, and Mach number, and are strongly affected by atmospheric disturbances such as turbulence, wind shear, icing, and wake-vortex encounters, which can simultaneously excite pitch, roll, and yaw motion and increase load factor [1,4].

1.2. Aerodynamic strength, Mach number and load factor

Aerodynamic strength and controllability are directly affected by aircraft speed, altitude, Mach number, and load factor. As altitude and temperature change, the local speed of sound also changes; therefore, the Mach number may vary even when the aircraft's true airspeed remains nearly constant [1–4].

$$M = \frac{V_{TAS}}{a} \tag{1}$$

where M is the Mach number, V_{TAS} is the true airspeed, and a is the local speed of sound [1,2].

The Mach number is directly linked to the aerometric method of airspeed measurement. In a pitot-static system, the dynamic (impact) pressure is defined as

$$\Delta p = p_t - p \tag{2}$$

where p_t is total pressure and p is static pressure.

Accounting for air compressibility at flight speeds, the Mach number can be expressed directly in terms of the measured dynamic pressure, where k is the specific heat ratio of air [1,2]. This relation is significant for the proposed approach because

Δp is the physical quantity measured directly by the smart aerometric probes described in Section 3.

$$M = \sqrt{\frac{2}{k-1}\left[(1+\frac{\Delta p}{p})^{\frac{k-1}{k}} - 1\right]}. \quad (3)$$

where Δp is the dynamic pressure, p_t is the total pressure measured by the pitot tube, p is the static pressure, M is the Mach number, and k is the specific heat ratio of air [1,2].

The flight Mach number is used to classify the airflow regime around an aircraft. At low subsonic speeds, the airflow can be treated as nearly incompressible. As the Mach number increases, compressibility effects become more important. When the aircraft approaches the critical Mach number, some local regions of the flow may reach sonic speed, and shock waves may begin to form [1–4].

The main flow regimes can be described as follows: low subsonic flow occurs at $M < 0.4$, where compressibility effects are usually small. High subsonic flow occurs at $0.4 < M < M_{crit}$, where the airflow remains subsonic but compressibility becomes important. Transonic flow begins near or above M_{crit}, when both subsonic and local supersonic regions may exist around the aircraft. Supersonic flow occurs when the flow is generally above $M = 1.0$. Hypersonic flow occurs at $M > 5$, where very strong compressibility effects, shock-wave interactions, and aerodynamic heating become dominant factors [1–4].

For transport aircraft, high cruise speed is operationally beneficial. However, flight above the critical Mach number can lead to shock-wave formation and a rapid drag increase. This additional drag is known as wave drag and is mainly associated with energy losses and boundary-layer separation. The Mach number at which drag starts to increase rapidly is called the drag-divergence Mach number, which is usually close to, but higher than, the critical Mach number [1–4].

Mach number influences aerodynamic behavior, compressibility effects, control-surface effectiveness, and stability margins [1, 3]. At the same time, maneuvering flight, turbulence, gusts, or wake-vortex encounters may increase the load factor [1–4]:

$$n = \frac{L}{W} \quad (4)$$

where n is the load factor, L is lift, and W is aircraft weight.

When the load factor increases or when the aircraft operates close to aerodynamic limits, the available control margin may decrease. This can make the aircraft more sensitive to disturbances and may increase oscillatory motion in pitch, roll, and yaw channels. Therefore, Mach number, sound speed, and load factor must be considered before analyzing aircraft stability and controllability under disturbed atmospheric conditions [2–4].

2. Stability and controllability under disturbed atmospheric conditions

Aircraft controllability and stability are two fundamental, but opposite characteristics of flight dynamics. Stability describes the tendency of an aircraft to return to its equilibrium condition after a disturbance, whereas controllability describes the ability of the pilot or automatic flight-control system to change the aircraft's attitude and trajectory as required. In general, increasing stability improves the natural resistance of the aircraft to disturbances, but may reduce maneuverability and response speed. Conversely, increasing controllability can improve maneuvering capability, but may also increase sensitivity to pilot inputs, atmospheric disturbances, and oscillatory motion [2–4].

This balance becomes especially important under disturbed atmospheric conditions. Turbulence, wind gusts, wake-vortex encounters, wind shear, icing, and system failures can disturb the aircraft's motion in pitch, roll, and yaw channels. If these disturbances are not corrected in time, they may increase transient deviations, reduce damping, and create conditions that can contribute to loss of control in flight [2–4,6]. Although commercial aviation accident rates have decreased over recent decades, Boeing Commercial Airplanes [6] still identifies LOC-I (Loss of Control—Inflight) among the principal fatal-accident occurrence categories for the worldwide commercial jet fleet in 2015–2024. This confirms that aircraft controllability, stability margins, and disturbance response remain relevant safety-related research topics.

As shown in **Table 1**, although the overall accident, hull-loss, and fatal accident rates have decreased over the last two decades, LOC-I remains one of the most severe fatal-accident categories in terms of onboard fatalities. Therefore, improving aircraft controllability, stability margins, and disturbance response remains an important safety-related research direction.

Table 1. Boeing accident statistics supporting the continued relevance of aircraft stability and controllability research [6].

Parameter/Category	Period	Boeing statistical data	Relevance to this study
Accident rate trend	Last two decades	40% decline in total accident rate	Safety motivation
Hull-loss rate trend	Last two decades	55% decline in hull-loss rate	Severity reduction
Fatal accident rate trend	Last two decades	65% decline in total accident rate	Fatal-risk context
Departures	Last two decades	23% increase in departures	Growing exposure
Total commercial jet accidents	2015–2024	298 total accidents	Ongoing risk
Fatal accidents	2015–2024	30 fatal accidents	Safety-critical issue
Hull-loss accidents	2015–2024	90 hull-loss accidents	Severe outcomes
Onboard and external fatalities	2015–2024	982 onboard fatalities and 66 external fatalities	Human-safety impact
LOC-I	2015–2024	6 fatal accidents, 428 onboard fatalities	Direct control relevance

Conventional flight-control and stability-augmentation systems operate with a finite stability margin. In control-system analysis, this margin is commonly evaluated through phase margin and gain margin [7–9].

Under severe turbulence, wind shear, wake-vortex encounter, or abnormal system conditions, the aircraft may experience rapid pitch, roll, and yaw deviations. The autopilot and stability-augmentation system must keep sufficient robustness despite changing aerodynamic conditions.

Sometimes severe turbulence, excessive attitude deviations, pilot override, flight-envelope protection activation, or system failures may lead to autopilot disengagement or require manual control, depending on the aircraft type and system logic. When manual control is required under disturbed atmospheric conditions, pilot workload increases. The pilot must control the aircraft, monitor flight parameters, follow abnormal procedures, and react to external disturbances at the same time. This may increase the probability of human-factor errors [6, 10–12].

Therefore, adaptive modification of phase and gain margins under disturbed atmospheric conditions may improve the robustness of the flight-control system [10–12]. In this study, aerometric smart-probe information is proposed as an additional input for earlier disturbance detection and adaptive correction of aircraft rotational motion [10–15].

Vortex disturbance and its influence on pitch, roll, and yaw motions

Wake-vortex disturbance is one of the important external atmospheric hazards that can significantly affect aircraft stability and controllability, especially during takeoff, approach, and landing, when the aircraft operates at low altitude. A wake vortex generated by a preceding aircraft may create strong local airflow asymmetry and vertical gust components, which can disturb the aircraft in pitch, roll, and yaw channels simultaneously [2–4].

Among these motions, pitch disturbance may be considered the most dangerous at low altitude, because a sudden nose-down response can rapidly reduce the flight-path angle and altitude, increasing the risk of ground impact before the crew or automatic control system can fully compensate for the deviation. Roll and yaw disturbances are also dangerous, particularly during takeoff and landing, because they can cause lateral-directional deviation from the runway centerline, increase sideslip, and in severe cases lead to runway excursion or loss of directional control [2–4, 16, 17].

Therefore, wake-vortex influence should be considered as a critical disturbance source in the analysis of aircraft stability and controllability under disturbed atmospheric conditions. In this study, the wake-vortex effect is represented as a transient vertical-gust input, as shown in **Figure 1**.

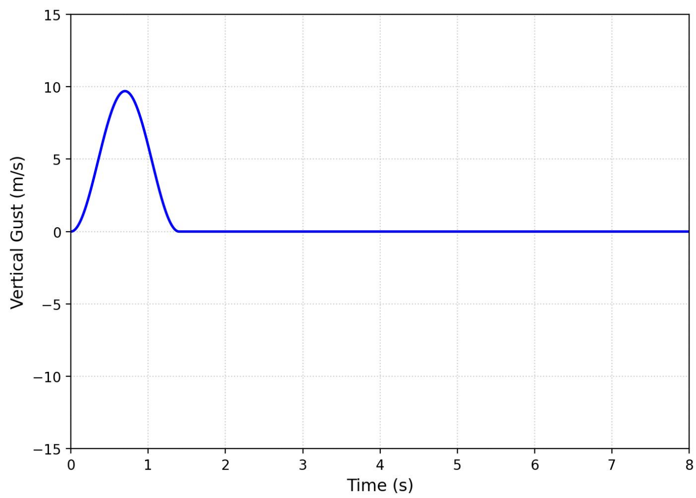

Figure 1. Wake-vortex disturbance profile used in the simulation (vertical gust component).

As shown in **Figure 1**, the wake-vortex disturbance is represented as a time-domain vertical-gust input with a limited effective duration. This disturbance profile is used in the present study as an external input for evaluating the transient response of the aircraft in the pitch, roll, and yaw channels under disturbed atmospheric conditions.

Because pitch motion directly affects flight-path angle, load factor, and altitude safety margin, the pitch channel is analyzed first in the following section.

The proposed aerometric approach for measuring aerometric disturbance in aircraft is based on the placement of pressure probes at several aircraft locations, including the nose section, wingtips, and tail section. The general arrangement of the pressure probes is shown in **Figure 2** [15].

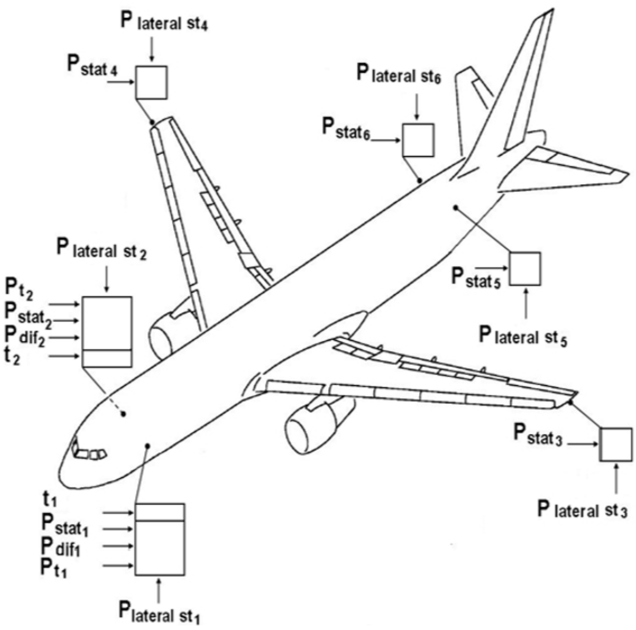

Figure 2. Layout of pressure probe locations in the proposed aerometric assisted improvement system.

3. Pitch channel stability, oscillatory motion, and controllability

Pitch motion is a main part of aircraft longitudinal dynamics and is mainly controlled by the elevator or stabilizer. It directly affects angle of attack, flight path, load factor, and stall margin. Under turbulence, gusts, or wake-vortex influence, the pitch channel may experience increased oscillations and transient deviations [10, 11].

The conventional pitch-rate damper is based on gyroscopic feedback. In this structure, the pitch-rate gyro measures the developed pitch-rate response, and the pitch-rate controller generates an elevator command through the elevator actuator to damp the oscillatory motion [7, 8, 10, 11].

As shown in **Figure 3**, the controller begins correction only after the pitch-rate deviation has already appeared. Therefore, under turbulence, gusts, or wake-vortex disturbance, the aircraft may first experience increased pitch oscillation before the damping action becomes effective. This limitation motivates the use of additional aerometric information for earlier disturbance detection and adaptive correction [10–15].

Since wake-vortex disturbance contains a vertical-gust component, it can directly influence the longitudinal motion of the aircraft. In the pitch channel, such a disturbance may change the angle of attack, flight-path angle, and altitude safety margin. Therefore, before introducing the proposed aerometric-assisted correction, the conventional pitch-control feedback structure should be considered.

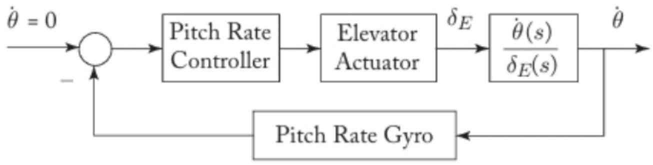

Figure 3. Simplified conventional pitch-rate damper architecture based on gyroscopic feedback.

The pitch-angle control system can be represented as a feedback structure with two control loops. The inner loop uses pitch-rate feedback to improve damping and suppress short-period oscillations, while the outer loop uses attitude-angle feedback to maintain the required pitch attitude. This structure improves longitudinal stability compared with a single feedback loop; however, the correction begins after the pitch-rate or pitch-angle deviation has already developed [1].

As shown in **Figure 4**, the pitch-control system uses both rate-gyro and attitude-gyro feedback. The inner rate loop increases damping of pitch oscillations, whereas the outer attitude loop reduces steady pitch-angle error and supports attitude tracking. However, this architecture does not directly measure the incoming airflow disturbance. Therefore, during a wake-vortex encounter, the aircraft may first experience pitch deviation before the feedback system generates the corrective elevator command.

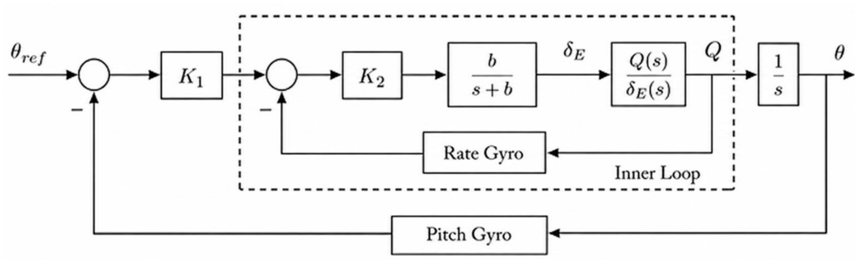

Figure 4. Simplified block diagram of the pitch-angle control system with inner pitch-rate feedback and outer attitude-angle feedback.

The importance of pitch-channel stability becomes more evident when it is connected with altitude control. In a basic altitude-control system, the elevator command changes the aircraft's longitudinal dynamics, which affects the altitude response. Therefore, a wake-vortex-induced pitch disturbance can also produce an altitude deviation, especially when the aircraft operates at low altitude during approach or landing [1].

As shown in **Figure 5**, altitude control depends on the elevator servo, aircraft longitudinal dynamics, and altimeter feedback. A disturbance in the pitch channel can therefore propagate into the altitude-control loop. At low altitude, this is especially critical because even a short nose-down transient response may reduce the available altitude margin. This explains why pitch disturbance is considered more dangerous than roll and yaw disturbances during low-altitude wake-vortex encounters. Roll and yaw deviations may cause runway-centerline deviation or runway excursion, whereas severe pitch deviation may directly increase the risk of ground impact [1,2,4].

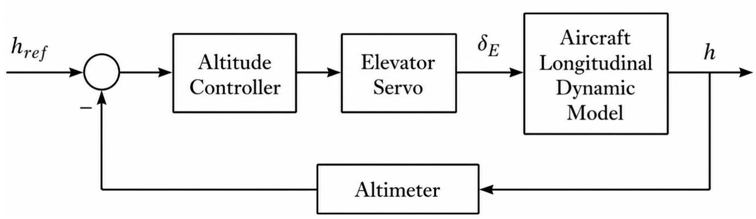

Figure 5. Simplified altitude-control system showing the relationship between elevator deflection, longitudinal dynamics, and altitude feedback.

The pitch-motion dynamics can be represented by the following second-order differential equation [2,4,11,18]:

$$\ddot{\theta} + 2\zeta\omega_n\dot{\theta} + \omega_n^2\theta = K_\theta\delta_E \tag{5}$$

Where,
θ is the pitch angle (rad),
$\dot{\theta}$ is the pitch angular rate (rad/s),
ζ is the damping ratio,
ω_n is the natural frequency,
δ_E is the elevator deflection angle,
K_θ is the pitch-control effectiveness coefficient.

This mathematical representation shows that the conventional pitch-rate damper is mainly based on the measured pitch response and elevator feedback. Although this structure can damp pitch oscillations, its corrective action begins only after the pitch-rate deviation has already developed. Under atmospheric disturbances, such as turbulence, gusts, or wake-vortex encounters, this delay may increase the transient pitch response and reduce the available stability margin. Therefore, an additional information source is required to detect disturbance development earlier and support faster pitch-channel correction. Based on this limitation, the following subsection introduces the aerometric-assisted pitch-channel stability augmentation concept [10–15].

3.1. Practical feasibility of aerometric sensing

The practical implementation of the proposed aerometric-assisted approach depends on the dynamic characteristics of the smart aerometric probes. Modern pressure-based smart probes typically offer response times in the range of a few milliseconds to tens of milliseconds, which is significantly faster than the characteristic time scales of aircraft rotational dynamics considered in this study. Pressure resolution on the order of tens of pascals is achievable with current MEMS-based and pitot-static sensor technology, sufficient to detect pressure variations from gusts and wake-vortex encounters before they translate into significant angular motion. Installation on the wingtips and tail section requires structural integration and periodic calibration against reference pitot-static systems. A detailed sensor-level uncertainty and calibration analysis is beyond the scope of this conceptual study and is identified as a step toward flight-hardware implementation.

3.1.1. Aerometric-assisted pitch-channel stability augmentation concept

The proposed approach is based on the use of aerometric smart-probe information as an additional input to the conventional stability-augmentation system. In a classical feedback structure, the control system reacts after angular motion has already appeared. In the proposed structure, pressure-based aerometric signals provide earlier information about airflow asymmetry and external disturbances [13–15].

To illustrate the proposed pitch-channel concept, the principle structure of the aerometric-assisted pitch-stability control system is shown in **Figure 6**.

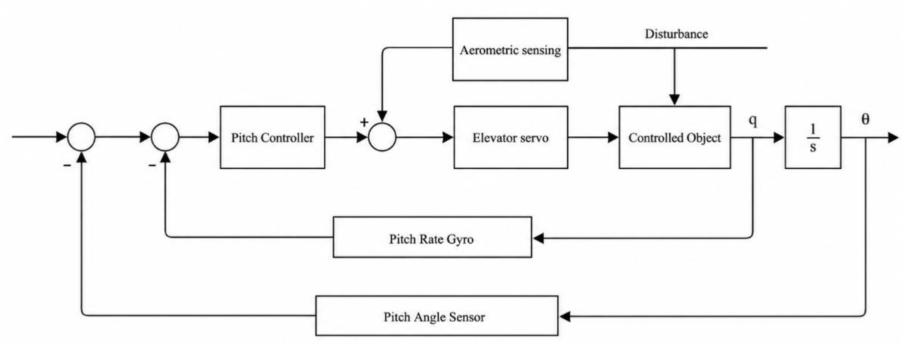

Figure 6. Principle structure of the aerometric-assisted pitch-stability control system.

As shown in **Figure 6**, the proposed pitch-stability system combines several feedback and compensation paths. The pitch controller generates the basic elevator command, while the elevator servo represents the actuator dynamics. The controlled object describes the aircraft's longitudinal pitch response. The pitch-rate gyro and pitch-angle sensor provide conventional and modern feedback information, whereas the aerometric sensing block detects airflow disturbance before the pitch deviation becomes fully developed.

This architecture is important because pitch disturbances may develop rapidly under wake-vortex, gust, or asymmetric airflow conditions. In a conventional feedback loop, the controller reacts mainly after pitch motion has appeared. In the proposed structure, the aerometric channel provides additional disturbance-related information and supports earlier corrective action. This can reduce pitch-angle deviation, suppress oscillation amplitude, and improve transient damping under disturbed atmospheric conditions.

The aerometric channel is not intended to replace gyroscopic or inertial sensors [13–15]. Instead, it works as an additional feedback and preview-information source. This allows the controller to adapt its response before large pitch, roll, or yaw deviations develop.

In this study, the adaptive correction is implemented through modified controller gains under disturbed atmospheric conditions. The objective is to increase phase and gain margins, reduce oscillation amplitude, and shorten the transient response in aircraft rotational motion.

The general structure of the proposed aerometric-assisted stability augmentation system is shown in **Figure 7**.

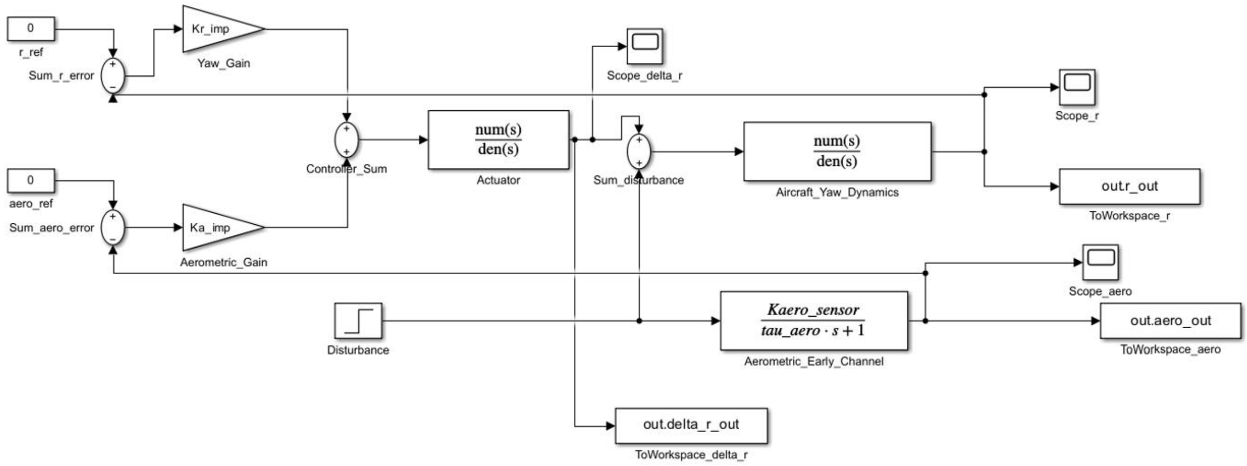

Figure 7. Proposed aerometric-assisted stability augmentation architecture.

As shown in **Figure 7**, the proposed architecture combines the conventional angular-rate feedback loop with an additional aerometric channel. The aerometric signal is used to detect airflow disturbance earlier and to support adaptive correction of the control command. This structure allows the system to improve damping and reduce transient rotational deviations under disturbed atmospheric conditions.

Compared with the conventional pitch-rate damper, the modified structure includes an additional disturbance path. The pitch-rate controller still generates the main elevator command based on gyroscopic feedback, while the disturbance input represents an external acceleration or airflow perturbation acting on the pitch channel. This configuration is used to evaluate how the controller responds when the aircraft is exposed to disturbed atmospheric conditions.

$$W_q(s) = \frac{\dot{\theta}(s)}{\delta_E(s)} = \frac{K_\theta}{s^2 + 2\zeta\omega_n s + \omega_n^2}. \tag{6}$$

where $W(s)$ is the pitch-angle transfer function, $\dot{\theta}(s)$ is the pitch-angle output, $\delta_E(s)$ is the elevator deflection input, and s is the Laplace operator, K_θ is the pitch-control effectiveness coefficient, ζ is the damping ratio, and ω_n is the natural frequency.

Since the final response is evaluated in terms of pitch angle, the pitch angle is obtained by integrating the pitch-rate response:

$$\theta(s) = \frac{\dot{\theta}(s)}{s}. \tag{7}$$

In this study, the pitch-channel response is analyzed by comparing the conventional feedback controller with the proposed aerometric-assisted adaptive controller. The objective is to evaluate whether the additional aerometric information can reduce pitch oscillation amplitude and shorten the transient response under disturbed atmospheric conditions [10, 11].

3.1.2. Pitch-angle response comparison

The pitch-angle response was compared for three stability-augmentation approaches: the conventional controller, the modern controller, and the proposed aerometric-assisted controller. The comparison was performed under the same disturbed atmospheric conditions in order to evaluate the influence of the control architecture on pitch-angle deviation, oscillation amplitude, and transient damping.

The response curves shown in **Figure 8** were obtained from the simulation models developed based on the control architectures presented in **Figures 3**, **4**, and **6**.

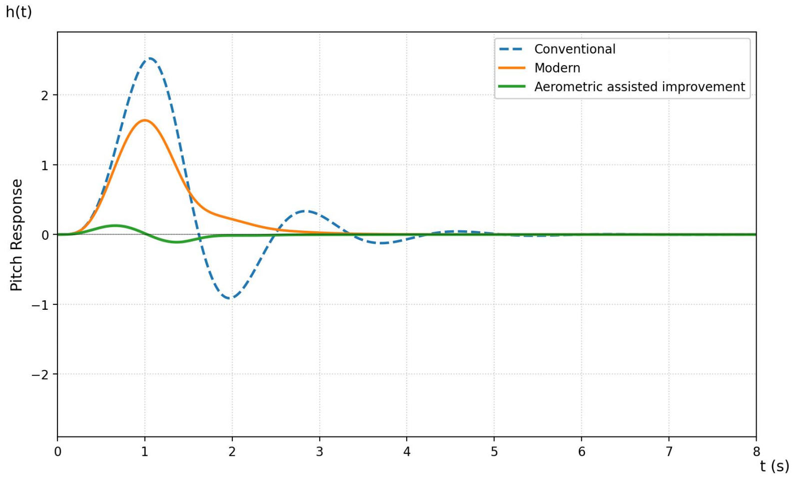

Figure 8. Pitch-angle response comparison of the conventional, modern, and aerometric-assisted stability augmentation approaches.

As shown in **Figure 8**, the conventional approach exhibits the largest pitch-angle oscillation amplitude and the slowest damping response. The modern approach improves the transient behavior by reducing both the maximum pitch deviation and the oscillation amplitude. However, the proposed aerometric-assisted approach appears to provide a more favorable transient response, with visibly lower pitch-angle deviation and reduced oscillation amplitude compared with the other two architectures under the disturbance condition considered. These qualitative observations suggest that the additional aerometric disturbance information may improve pitch-channel damping. A quantitative case study confirms this trend: under the design gust considered (see Section 7), the aerometric-assisted architecture reduces peak pitch-angle deviation by 94.9% relative to the conventional approach and by 92.2% relative to the modern approach, using gains selected under identical stability-margin and control-effort constraints for all three architectures.

4. Roll channel stability and controllability

Roll motion is a main part of aircraft lateral dynamics and is mainly controlled by ailerons or spoilers. It directly affects bank angle, maneuvering capability, lateral stability, and flight-path control. Under turbulence, gusts, or wake-vortex encounters, the roll channel may experience rapid angular deviations because external airflow disturbances can generate additional rolling moments [19–21].

The conventional roll-rate damper is based on gyroscopic feedback. In this structure, the roll-rate gyro measures the developed roll-rate response, and the roll-rate controller generates an aileron command through the aileron actuator to damp lateral oscillatory motion [19–21].

As shown in **Figure 9**, the conventional roll-rate damper operates as a feedback system. The controller begins correction only after the roll-rate deviation has already appeared. Therefore, under turbulence, gusts, or wake-vortex disturbance, the aircraft may first experience increased roll deviation before the damping action becomes effective [7,12,19,21].

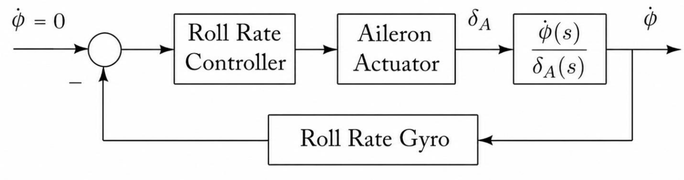

Figure 9. Simplified conventional roll-rate damper architecture based on gyroscopic feedback.

$$W_{\dot{\phi}}(s) = \frac{\dot{\phi}(s)}{\delta_A(s)} = \frac{K_\phi}{s^2 + 2\zeta_\phi \omega_{\phi n} s + \omega_{\phi n}^2}. \tag{8}$$

where $W_{\dot{\phi}}(s)$ is the roll-rate transfer function, $\dot{\phi}(s)$ is the roll-rate output, $\delta_A(s)$ is the aileron deflection input, s is the Laplace operator, K_ϕ is the roll-control effectiveness coefficient, ζ_ϕ is the roll-channel damping ratio, and $\omega_{\phi n}$ is the roll-channel natural frequency.

$$\phi(s) = \frac{\dot{\phi}(s)}{s}. \tag{9}$$

Since the final response is evaluated in terms of roll angle, the roll angle is obtained by integrating the roll-rate response.

This conventional structure provides the baseline roll-channel model. However, it does not use direct airflow-disturbance information. Therefore, the roll channel was further analyzed using an aerometric-assisted roll-stability architecture, where an additional aerometric sensing path is introduced to support earlier detection of lateral airflow asymmetry [13–15,19].

This section extends the previous roll-angle response comparison by showing the internal control-loop structure, the corresponding MATLAB/Simulink implementation, and the time-domain behavior of the main system signals [20,21].

Roll stability is affected not only by the roll angle itself, but also by roll rate, sideslip-related lateral motion, actuator delay, sensor dynamics, and external airflow disturbances. Therefore, the proposed roll-stability architecture includes a conventional roll controller, an aileron servo, the controlled aircraft roll dynamics, roll-rate feedback, sideslip-angle feedback, and an additional aerometric sensing channel [19–21].

In addition to the conventional roll-rate damper, the roll channel can be represented by a two-loop roll-angle control structure. In this architecture, the inner loop uses roll-rate feedback to improve damping, while the outer loop uses roll-angle feedback to maintain the required bank angle and improve attitude tracking [1].

As shown in **Figure 10**, the modern roll-control structure provides better damping and bank-angle regulation than the conventional roll-rate damper. However, a corrective aileron command is generated only after a speed or bank angle deviation has already occurred. Therefore, an additional aerometric measurement channel is introduced into the proposed roll stabilization architecture.

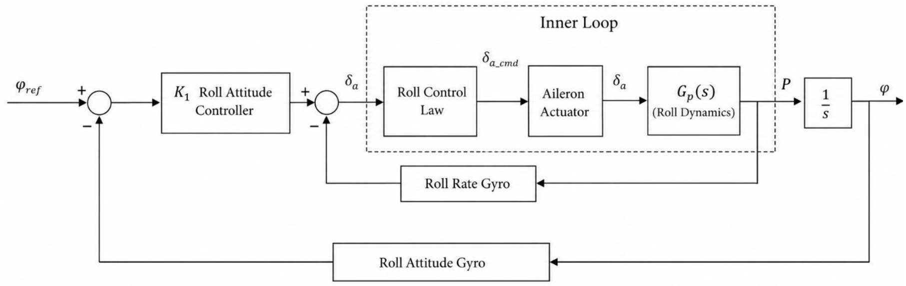

Figure 10. Simplified block diagram of the roll-angle control system with inner roll-rate feedback and outer roll-angle feedback.

The principal structure of the aerometric-assisted roll-stability control system is shown in **Figure 11**.

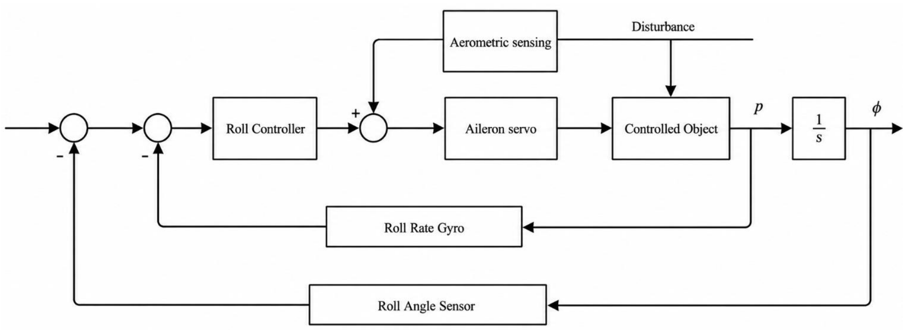

Figure 11. Principle structure of the aerometric-assisted roll-stability control system.

As shown in **Figure 11**, the proposed roll-stability system combines several feedback and compensation paths. The roll controller generates the basic aileron command, while the aileron servo represents the actuator dynamics. The controlled object describes the aircraft's roll response. The roll-rate gyro and roll-angle sensor provide additional lateral-directional feedback, and the aerometric sensing block detects airflow disturbance before the roll deviation becomes fully developed.

This architecture is important because roll disturbances may develop rapidly under wake-vortex, gust, or asymmetric airflow conditions. In a conventional and modern architecture, the controller reacts mainly after the roll motion has appeared. In the proposed structure, the aerometric channel provides additional disturbance-related information and supports earlier corrective action [15,19–21].

The main dynamic blocks used in the MATLAB Simulink model are represented by first-order transfer functions:

$$G_s(s) = \frac{K_A}{T_A s + 1} \tag{10}$$

$$G_p(s) = \frac{K_R}{T_R s + 1} \tag{11}$$

$$G_r(s) = \frac{K_g}{T_g s + 1} \tag{12}$$

$$G_\phi(s) = \frac{K_\phi}{T_\phi s + 1} \tag{13}$$

Here, $G_s(s)$ represents the aileron servo dynamics, $G_p(s)$represents the controlled roll-dynamic object, $G_r(s)$represents the roll-rate gyro dynamics, and $G_\phi(s)$ represents the roll-angle sensor dynamics. These transfer functions describe the main delays and gains inside the roll-stability control loop [7,8].

The corresponding MATLAB/Simulink implementation of the aerometric-assisted roll-stability system is presented in **Figure 12.**

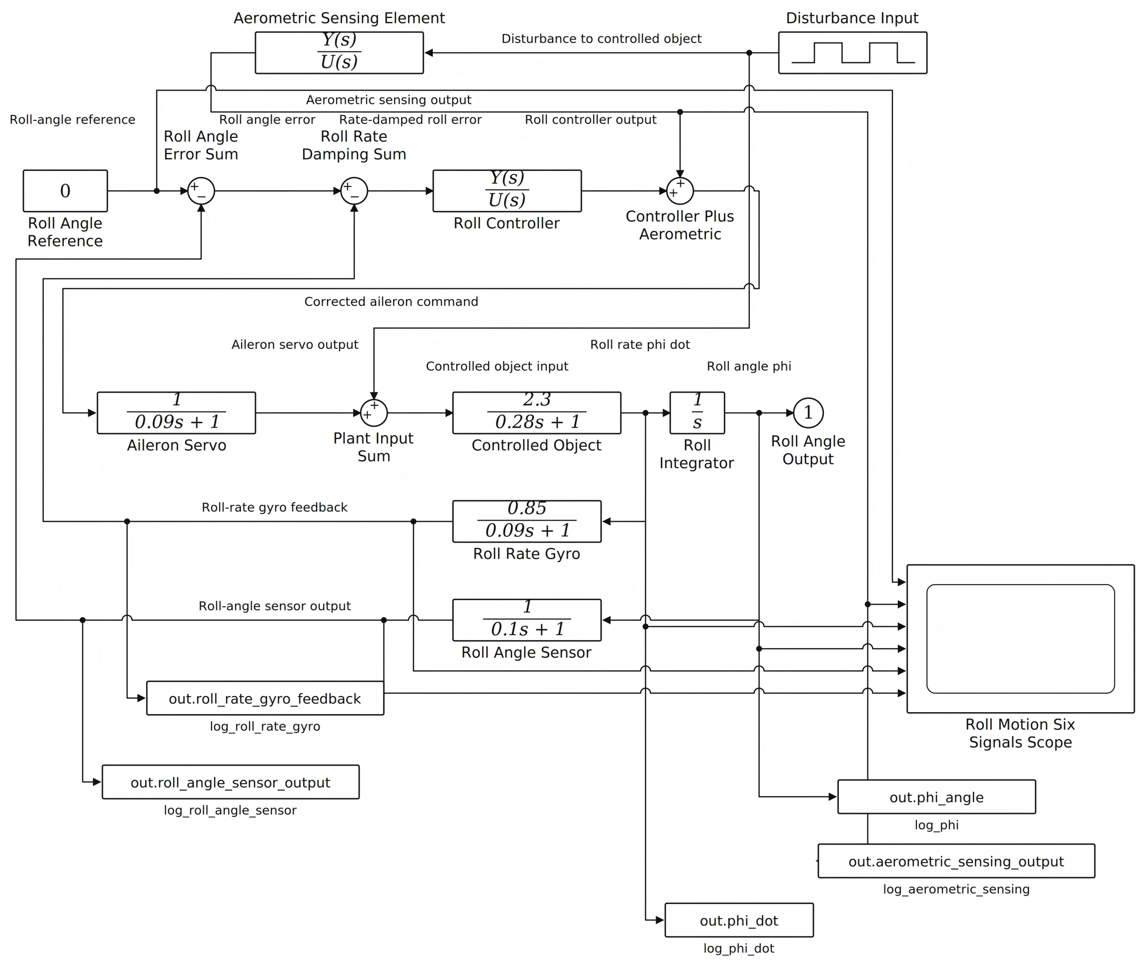

Figure 12. MATLAB/Simulink model of the aerometric-assisted roll-stability control system.

As shown in **Figure 12**, the Simulink model includes the reference roll-angle input, roll controller, aileron servo, controlled object, roll-rate gyro, roll-angle sensor, sideslip feedback path, and aerometric sensing output. This model allows the internal signals of the roll-stability system to be observed simultaneously. Therefore, the behavior of the controller can be evaluated not only by the final roll-angle output, but also by the response of the sensor and feedback channels [19–21].

Roll stability is especially important during atmospheric disturbance encounters because lateral airflow asymmetry can rapidly create rolling moments. In wake-vortex or gust conditions, the aircraft may experience sudden bank-angle changes, which require fast and well-damped control action. Therefore, the roll-channel simulation is used to evaluate how the proposed aerometric-assisted controller affects lateral response and transient roll behavior [19–21].

The roll-angle response was compared for three control approaches: the conventional feedback controller, the modern controller, and the proposed aerometric-assisted controller. The comparison was performed under the same aerometric disturbance condition in order to evaluate the influence of each control structure on bank-angle deviation, oscillation amplitude, and transient damping.

The roll-angle response curves shown in **Figure 13** were obtained from simulation models developed based on the classical, modern, and proposed roll-control architectures presented in **Figures 9–11**, respectively.

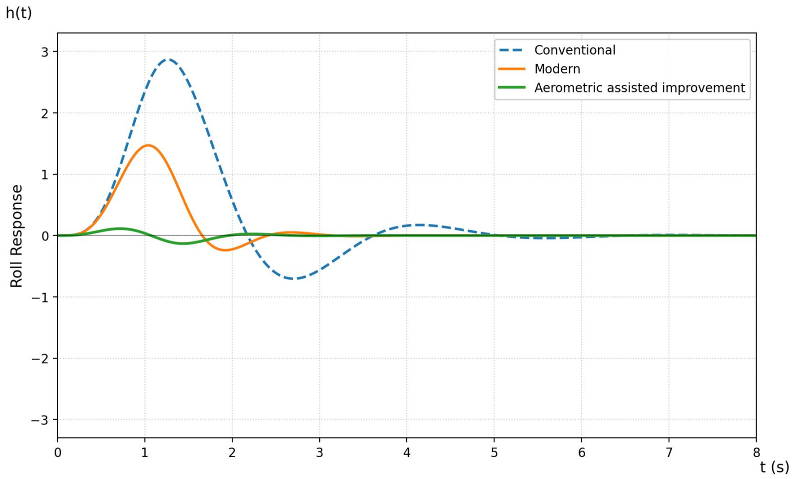

Figure 13. Roll-angle response comparison of the conventional, modern, and proposed aerometric-assisted stability augmentation approaches.

As shown in **Figure 13**, the conventional controller produces the largest bank-angle deviation and the slowest damping response. The modern controller reduces the roll-angle amplitude and improves the transient behavior compared with the conventional approach. However, the proposed aerometric-assisted controller appears to provide a more favorable response, with visibly smaller bank-angle deviation compared with the other two architectures under the disturbance condition considered. This observation suggests that the additional aerometric information may improve roll-channel damping and lateral controllability. A quantitative case study confirms this trend: peak roll-angle deviation is reduced by 95.4% relative to the conventional approach and by 91.0% relative to the modern approach (see Section 7).

5. Yaw channel stability and aerometric disturbance detection

Yaw motion is a key part of aircraft directional stability and is mainly controlled by the rudder. It affects sideslip angle, coordinated flight, and lateral-directional stability. Under turbulence, crosswind, wake-vortex influence, or asymmetric airflow conditions, the yaw channel may experience unwanted directional deviations [19–21].

The yaw channel was additionally analyzed through the yaw-damper architecture because directional stability is strongly affected by lateral airflow asymmetry, sideslip, crosswind, and wake-vortex influence. The classical and modern yaw damper to prevent Dutch-roll mainly uses the yaw rate feedback from the gyroscopic sensor and generates a rudder command after the yaw motion has already occurred [19–21].

The basic yaw-damper control loop is shown in **Figure 14**.

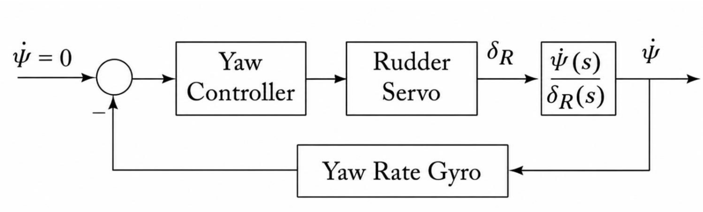

Figure 14. Classical gyroscope-based yaw-damper architecture.

As shown in **Figure 14**, the classical yaw damper is based on a feedback structure in which the yaw-rate gyro measures the developed yaw motion and sends this signal to the controller. The controller then generates a rudder command to damp the yaw oscillation. This architecture is effective for Dutch-roll damping, but its corrective action begins only after the yaw-rate response has already developed [19–21].

To reduce this delay, the proposed architecture adds an aerometric smart-probe channel to the conventional yaw-rate feedback loop. The aerometric channel does not replace the gyroscope. Instead, it provides additional pressure-based information about lateral airflow asymmetry before the yaw deviation becomes fully developed [13–15].

Although the yaw channel can be studied separately through a classical yaw damper, in practical flight-control systems it is commonly integrated into the lateral-directional stability augmentation system (SAS), where roll and yaw motions are controlled simultaneously through coupled feedback loops.

As shown in **Figure 15**, the conventional lateral-directional SAS includes both roll and yaw feedback channels. The upper loop uses roll-rate feedback to support roll stabilization, whereas the lower loop uses yaw-rate feedback to improve directional stability and damp yaw oscillations. In the present study, the main focus is placed on the yaw channel, because directional disturbances caused by crosswind, wake-vortex, and airflow asymmetry can strongly affect aircraft yaw stability and controllability.

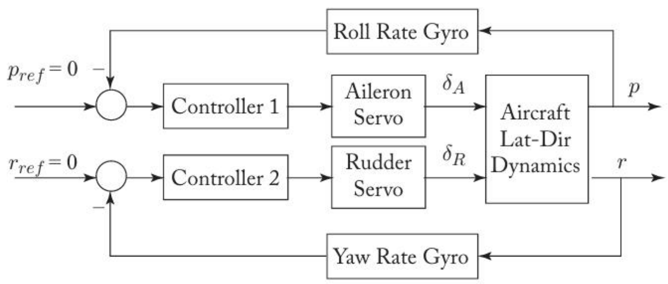

Figure 15. Conventional lateral-directional stability augmentation system (SAS) with roll-rate and yaw-rate feedback loops.

The enhanced yaw-damper architecture is shown in **Figure 16**.

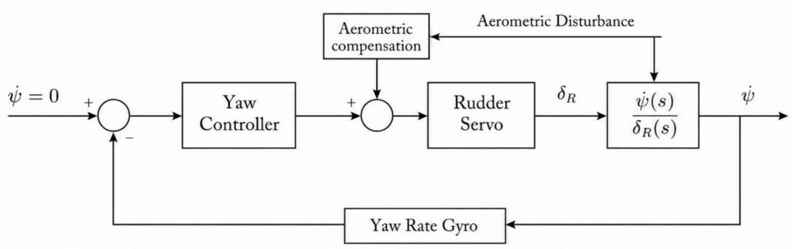

Figure 16. Simplified aerometric smart-probe-assisted yaw-damper architecture.

As shown in **Figure 16**, the enhanced yaw-damper system combines two information sources: gyroscopic yaw-rate feedback and considering aerometric disturbance pressure-based influence. The gyroscope measures the actual yaw motion, while the aerometric smart probe detects lateral pressure differences caused by airflow asymmetry. This allows the controller to receive earlier disturbance information and generate a faster rudder correction [13–15, 19–21].

The aerometric channel can be represented as a first-order pressure-based element [15]:

$$G_{\text{aero}}(s) = 1/\left(\tau_{\text{aero}} \cdot s + 1\right) \tag{14}$$

where τ_{aero} is the aerometric sensor time constant. Taking into account the atmospheric disturbance factor with a shorter sensor time constant allows the aerometric channel to provide information about disturbances earlier than the traditional inertial feedback loop.

The combined yaw-damper control command can be expressed as:

$$u(t) \;=\; -K_r \cdot r(t) \;-\; K_a \cdot a_{\text{aero}}(t) \tag{15}$$

where $r(t)$ is the yaw angular rate measured by the gyroscope, $a_{\text{aero}}(t)$ is the aerometric signal, K_r is the gyroscopic feedback gain, and K_a is the aerometric channel gain.

In conventional and modern yaw-damper systems, correction is mainly based on yaw-rate or inertial feedback after the deviation has already appeared [19, 21]. In the proposed approach, the aerometric smart-probe signal provides earlier information about lateral airflow asymmetry. This allows the controller to support faster correction and reduce yaw oscillations [13–15].

The yaw-angle response comparison for the conventional, modern, and proposed aerometric-assisted control approaches is presented in **Figure 17**.

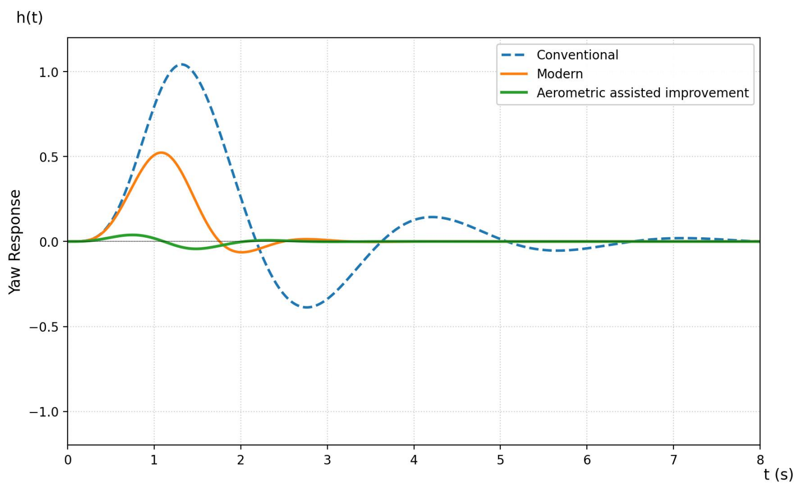

Figure 17. Yaw-angle response comparison of the conventional, modern, and proposed aerometric-assisted stability augmentation approaches.

As shown in **Figure 17**, the conventional controller produces the largest yaw-angle deviation and the most oscillatory response. The modern controller improves the transient behavior by reducing both the oscillation amplitude and the peak yaw deviation. However, the proposed aerometric-assisted controller appears to provide a more favorable overall response, with visibly smaller yaw-angle deviation and less oscillatory behavior compared with the other two architectures under the disturbance condition considered. These observations suggest that the additional aerometric information may improve yaw-channel stability and directional controllability. A quantitative case study confirms this trend: peak yaw-angle deviation is reduced by 95.9% relative to the conventional approach and by 91.7% relative to the modern approach (see Section 7).

5.1. Proposed adaptive gain-scheduling law

Since aerodynamic control-surface effectiveness scales approximately with dynamic pressure, the channel gain is proposed to be scheduled inversely with the aerometrically measured dynamic pressure Δp, and increased with load factor to reduce excess stability during maneuvering, consistent with standard dynamic-pressure gain-scheduling practice in flight control design [8]:

$$K(M,\ n,\ \Delta p)\ =\ K_0 \cdot (\Delta p_{\mathrm{ref}}/\Delta p) \cdot [1\ +\ \lambda(n\ -\ 1)] \tag{16}$$

where K_0 is the reference gain at the reference dynamic pressure Δp_{ref}, and $\lambda > 0$ is a maneuvering-sensitivity coefficient. To ensure smooth, causal adaptation compatible with the aerometric sensor dynamics of Equation (14), the gain increment $\Delta K(t)\ =\ K(t)\ -\ K_0$ is governed by the first-order adaptation law

$$\tau_K\ (d\Delta K/dt)\ +\ \Delta K(t)\ =\ K(M,\ n,\ \Delta p)\ -\ K_0 \tag{17}$$

where τ_K is the adaptation time constant. Equation (17) defines the adaptation dynamics for $K(t)\ =\ K_0\ +\ \Delta K(t)$ explicitly, reducing to the scheduled value $K(M,\ n,\ \Delta p)$ once transients in M, n, and Δp have settled.

5.2. General closed-loop stability analysis

Consider the representative case in which the channel actuator is modeled as a first-order lag $K_{\mathrm{a}}/(T_{\mathrm{a}}s\ +\ 1)$ (as already introduced in Equation (10) for the aileron servo) and the adaptive gain $K(t)$ is applied proportionally. Using the frozen-time approximation standard in gain-scheduled control analysis, the closed-loop characteristic equation is

$$T_a s^3\ +\ (2\zeta\omega_n T_a + 1)s^2\ +\ (\omega_n^2 T_a + 2\zeta\omega_n)s\ +\ (\omega_n^2\ +\ K(t)K_a K)\ =\ 0 \tag{18}$$

Applying the Routh–Hurwitz criterion, closed-loop stability requires

$$K(t)\ <\ [2\zeta\omega_n(T_a^2\omega_n^2\ +\ 2T_a\omega_n\zeta\ +\ 1)]/(T_a \cdot K_a \cdot K) \tag{19}$$

Equation (19) gives an explicit, analytically derived upper bound on the admissible adaptive gain for guaranteed closed-loop stability, expressed in terms of the plant and actuator parameters ($\zeta,\ \omega_n,\ T_a,\ K_a,\ K$). Once the actuator and sensor parameters for a given channel are specified, this bound can be evaluated numerically to define the admissible range for K_0 and λ in Equation (16).

6. Comparative summary of pitch, roll, and yaw results

The pitch, roll, and yaw channel analyses show that the conventional feedback-based control structures can damp angular deviations, but their correction mainly begins after the disturbance has already affected the aircraft motion. **Table 2** summarizes the main limitations of conventional feedback control and the corresponding improvements obtained with the aerometric-assisted approach [7,21].

Table 2. Comparative summary of conventional and aerometric-assisted control effects in pitch, roll, and yaw channels.

Channel	**Conventional/Modern limitations**	**Aerometric-assisted improvement**
Pitch	Reactive damping after pitch-rate deviation	Reduced pitch-angle oscillation
Roll	Delayed response to lateral disturbance	Lower roll-angle deviation
Yaw	Correction after yaw-rate development	Earlier directional correction
Overall stability	Limited disturbance preview	Improved transient damping

As shown in **Table 2**, the main advantage of the aerometric-assisted approach is not the replacement of conventional gyroscopic feedback, but the addition of earlier disturbance-related information. This additional information improves transient damping and reduces angular deviations in all three rotational channels [10–12,19,21].

For a closed-loop system with equivalent damping ζ and natural frequency ω_{n}, standard second-order performance indices can be evaluated analytically as settling time

$$t_s \;\approx\; 4/(\zeta\omega_n) \text{ (2\% criterion)}, \tag{20}$$

and percent overshoot

$$\%\mathrm{OS} \;=\; 100 \cdot \exp(-\zeta\pi/\sqrt{(1-\zeta^2)}). \tag{21}$$

These expressions define the quantitative methodology for evaluating settling time and overshoot once channel-specific ζ and ω_n are available from validated simulation data.

7. Representative numerical case study

The parameter values used below are representative/illustrative and serve to demonstrate the analytical framework of Section 5; they are independent of the three-channel simulation parameters reported later in this section.

The representative parameters used throughout this section are: ζ = 0.7, ω_n = 3 rad/s, plant gain K = 1, actuator time constant T_a = 0.1 s, actuator gain K_a = 1, and adaptive controller gain $K(t)$ = 10 (well within the stability bound of Equation (19)). **Table 3** summarizes the resulting closed-loop performance indices for this representative case.

Table 3. Closed-loop performance indices.

Index	**Value**
Settling time t_s (2%)	2.66 s
Peak time	0.92 s
Percent overshoot	26.6 %

Table 3. *Cont.*

Index	Value
Rise time (10–90%)	0.37 s
Integral square error/Absolute error (ISE/AE)	0.32/0.56 (integrated over 0–8 s)
Gain margin	16.0 dB
Phase margin	108.8°

Table 4 examines the robustness of this design under a ± 20% joint perturbation of the parameters ζ, ω_n, and T_a.

Table 4. Robustness under ±20% joint parameter perturbation—ζ, ω_n, T_a perturbed as $p = p_0(1 + \delta)$, $|\delta| \leq 0.2$.

δ	ζ	ω_n	T_a	Stable?	t_s (s)	%OS
−0.2	0.56	2.40	0.080	Yes	3.76	43.9%
−0.1	0.63	2.70	0.090	Yes	2.90	34.7%
0	0.70	3.00	0.100	Yes	2.66	26.6%
+0.1	0.77	3.30	0.110	Yes	2.06	19.7%
+0.2	0.84	3.60	0.120	Yes	1.89	14.0%

The system remains stable across the full ±20% range. As an independent check, the analytical stability bound of Equation (19) ($K(t) < 63.4$) was verified numerically by sweeping $K(t)$: the closed-loop system is stable up to $K(t) = 63$ and becomes unstable at $K(t) = 64$, confirming the analytical prediction to within 2%.

Table 5 validates the gain-scheduling law of Equation (16) across a set of representative flight conditions.

Table 5. Validation across representative flight conditions using the gain-scheduling law of Equation (16).

Condition	M	n	$K(M, n, \Delta p)$	t_s (s)	%OS
Low-speed cruise	0.4	1.0	22.5	3.44	47.7%
Mid-speed cruise	0.6	1.0	10.0	2.66	26.6%
High-speed cruise	0.8	1.0	5.6	2.32	17.3%
Maneuvering, 2 g	0.6	2.0	13.0	2.63	32.3%
Maneuvering, 3 g	0.7	3.0	11.8	2.66	30.0%

The proposed gain-scheduling law maintains stable, bounded closed-loop performance across the representative flight envelope, automatically compensating controller gain for dynamic-pressure and load-factor variation.

Using representative sensor time constants (τ_{aero} = 20 ms; conventional rate-gyro time constant T_g = 50 ms) and the aircraft's own rotational response time to reach a detectable (5%) deviation (≈114 ms for the representative plant), the aerometric channel is analytically predicted to detect a disturbance approximately 118 ms earlier than conventional inertial feedback for this representative case.

For comparison, **Table 6** benchmarks this design against a full-state-feedback Linear Quadratic Regulator (LQR) for the same representative plant.

Table 6. Comparison with a full-state-feedback LQR design (Q = diag(10,1), R = 1) for the same representative plant.

Metric	Proposed (*K* = 10)	LQR
t_s (s)	2.66	1.24
%OS	26.6%	0.0%
ISE/IAE (integral of absolute error)	0.32/0.56	0.24/0.40

Both designs use unity-direct current (DC)-gain precompensation so that ISE and IAE are compared on a like-for-like basis.

For this representative single-channel model, a full-state-feedback LQR design achieves tighter closed-loop tracking performance than the simple proportional adaptive-gain structure of Equation (18). This is expected: LQR requires full state (angle and rate) feedback, whereas the proposed architecture's advantage is earlier disturbance detection via the aerometric preview path rather than tighter pole placement. Note: this LQR design does not include the actuator lag T_a included in the proposed structure's model; a fully matched comparison is left for future work.

Applying a stochastic Dryden vertical-gust model (representative parameters: turbulence intensity σ_w = 2 m/s, scale length L_w = 300 m, airspeed V = 150 m/s, per the standard shaping-filter form in Stevens et al.'s study [8]), normalized so that the gust RMS equals σ_w, the closed-loop output RMS is 0.205 (normalized units). This value is computed analytically from the H_2 norm of the closed-loop system and is therefore independent of any random seed; a 300-run Monte-Carlo check gives 0.200 ± 0.020, confirming stable, bounded behavior under continuous stochastic turbulence in addition to the discrete transient-gust case of **Table 4.**

To document the three-channel comparative simulation of **Figures 8**, **13**, and **17**. **Table 7** reports the plant/sensor parameters, **Table 8** reports the resulting controller gains, and **Table 9** reports the disturbance model applied to all three channels. All gains in **Table 8** are obtained under an identical design rule: minimize disturbance-response ISE subject to all closed-loop poles being stable, a minimum closed-loop damping ratio of 0.30 (this closed-loop value is distinct from the open-loop plant damping ratio of 0.70 listed in **Table 7**), phase margin ≥ 45°, gain margin ≥ 6 dB, attitude-loop crossover frequency ≤ $1/(3T_a)$, peak control-surface deflection ≤ 15°, and peak deflection rate ≤ 60°/s—the same constraints for every channel and every architecture, so that no architecture is favored by an inconsistent design standard.

Table 7. Actuator, sensor, and plant dynamics used in the three-channel simulation.

Element	Transfer function	Note
Control-surface servo	$1/(0.09s + 1)$	Common to all channels
Rate gyro	$0.85/(0.09s + 1)$	Common to all channels
Attitude sensor	$1/(0.10s + 1)$	Common to all channels
Aerometric sensor	$1/(0.020s + 1)$	Common to all channels
Roll plant $G(s)$	$2.3/[s(0.28s + 1)]$	Measured (**figure 12**)
Pitch plant $G(s)$	$13.5/(s^2 + 4.2s + 9)$	ζ = 0.70, ω_n = 3.0 rad/s; representative [3,4]
Yaw plant $G(s)$	$2.25/(s^2 + 2.1s + 2.25)$	ζ = 0.70, ω_n = 1.5 rad/s; representative [3,4]

Table 8. Controller gains resulting from the design rule stated above.

Channel	K_c (conventional)	K_c (modern)	K_r (modern)
Pitch	0.689	0.653	0.50
Roll	0.854	2.013	0.50
Yaw	1.540	4.261	1.75

Table 9. Disturbance model applied to all three channels.

Parameter	Value
Gust type	discrete "1-cosine" (CS-25.341/MIL-HDBK-1797)
Design gust velocity, U_{ds}	9.7 m/s
Gust length	1.4 s
Gust-to-equivalent-deflection coupling, κ	0.30 deg/(m/s)

Only the roll-channel plant parameters are measured values, taken directly from the manuscript's own Simulink implementation; the pitch and yaw plant parameters are representative values selected from typical Level-1 handling-quality ranges, since no measured parameters exist for these two channels.

The aerometric-assisted architecture uses the same K_c and K_r as the modern architecture, plus a feed-forward path with approximate actuator-lag inversion, $G_{ff}(s)$ = $(T_a s + 1)/[K_a(T_{fs} + 1)]$, T_f = 20 ms, driven by the aerometric sensor output.

Code availability: The MATLAB script used to generate the representative case study of Section 7 and the three-channel comparative simulation of **Figures 8**, **13**, and **17** (including the constrained gain-search procedure and the feed-forward mismatch/robustness study) is provided as **Supplementary Material**.

8. Discussion

The obtained results show that the aerometric-assisted control concept improves the transient response in pitch, roll, and yaw channels. In all three channels, the conventional and modern feedback structure reacts mainly after the angular deviation has already appeared. This behavior can increase oscillation amplitude and prolong the damping process under turbulence, gusts, or wake-vortex encounters.

Mach-dependent effects should also be considered when interpreting the proposed aerometric-assisted concept. Recent studies on high-speed aircraft stability, Mach-dependent control metrics, transonic dynamic stability derivatives, and multidelta-wing configurations show that compressibility and flight-regime variation can significantly affect stability and control behavior [22–25]. Therefore, the proposed approach should be further evaluated under different Mach numbers, dynamic-pressure levels, and flight configurations.

The pitch-channel response is also connected with longitudinal dynamic stability, while wake-vortex encounters can introduce additional transient disturbances that affect aircraft attitude and recovery behavior. This supports the need to evaluate the proposed aerometric-assisted controller not only under nominal disturbance inputs, but also under wake-vortex and flight-regime-dependent conditions.

The proposed aerometric-assisted structure introduces pressure-based disturbance information as an additional input to the conventional and modern inertial feedback loop. This does not replace gyroscopic or inertial sensors, but supports earlier detection of airflow asymmetry and disturbance development. As a result, the controller can generate corrective action earlier and reduce the amplitude and the transient response time.

The pitch-channel results show improved longitudinal damping and reduced pitch-angle oscillation. The roll-channel results indicate lower roll-angle deviation and better lateral controllability. The yaw-channel results show improved directional stability due to earlier detection of lateral airflow asymmetry. Therefore, the proposed approach can improve aircraft stability and controllability under disturbed atmospheric conditions.

These results are based on the representative parameter set stated at the beginning of Section 7. The separate three-channel comparative simulation of **Figures 8**, **13** and **17** uses the parameter set of **Tables 7–9**, in which the roll-channel parameters are taken from the manuscript's own Simulink implementation, while the pitch and yaw parameters are representative values. Validation against measured flight data remains an important direction for future work.

It is also worth noting that modern autopilot and flight-control-computer designs already address disturbance-induced oscillations, typically treated as flexural oscillations of the longitudinal axis, through optimal or model-based control strategies. Two common approaches are (i) increasing the settling time and stiffness constant of the PID controller gains, and (ii) applying a sinusoidal-variation input to counteract periodic disturbance components. The aerometric-assisted architecture proposed in this study is intended to complement such flight-computer-level strategies by providing earlier disturbance information to the existing control loop, rather than replacing it; integrating the proposed aerometric feedback path with a specific autopilot implementation is left for future work.

Future extensions of this work may include the incorporation of data-driven and intelligent control techniques—such as neural-network-based adaptive control, fractional-order disturbance modeling, or symbolic/automated derivation of controller gains—to complement the classical control-theoretic treatment adopted here, alongside the stability, robustness, and multi-condition validation steps identified above [26–28].

9. Conclusion

This study proposed an aerometric-assisted stability augmentation concept for improving aircraft controllability and stability under disturbed atmospheric conditions. The main idea is to use smart aerometric information as an additional disturbance-detection source together with conventional and modern gyroscopic and inertial feedback.

The results show that the proposed approach reduces maneuvering amplitude and transient oscillation time in pitch, roll, and yaw channels. In the pitch channel, the aerometric-assisted controller reduces pitch-angle oscillation and improves longitudinal damping. In the roll channel, it decreases roll-angle deviation and improves lateral controllability. In the yaw channel, it supports earlier correction of directional motion by detecting lateral airflow asymmetry.

Overall, the proposed concept demonstrates, through comparative simulation, the potential of aerometric information to support earlier disturbance detection and adaptive correction of aircraft rotational motion. An explicit adaptive gain-scheduling law, a closed-loop stability analysis with an analytically derived and numerically verified stability bound, and a representative numerical case study including quantitative performance indices and robustness analysis have been presented (Sections 5 and 7). Validation against measured flight-test data, together with multi-condition flight-envelope validation, remains the focus of ongoing work.

Supplementary material: The supporting information can be downloaded at: https://zy-misc.oss-ap-southeast-1.aliyuncs.com/cest/2026-8-27/ADECP-4719-supplementary_material.docx.

Author contributions: Conceptualization and supervision, TK and AM; software and resources, EA and VK; validation, TK, AM and VK; formal analysis and editing, RG and EA; investigation and data curation, TK and AM; writing original draft preparation, TK, VK and RG; visualization, RG and EA. All authors have read and agreed to the published version of the manuscript.

Funding: This work received no external funding.

Institutional review board statement: Not applicable.

Informed consent statement: Not applicable.

Data availability statement: All data that support the findings of this study are included within the article.

Conflict of interest: The authors declare no conflict of interest.

AI use statement: The authors declare that no artificial intelligence (AI) tools were used in the preparation of this manuscript.

References

1. Sadraey MH. Aircraft Performance: An Engineering Approach. CRC Press; 2023.
2. Vepa R. Flight Dynamics, Simulation, and Control of Aircraft: For Rigid and Flexible Aircraft, 2nd ed. CRC Press; 2023. doi: 10.1201/9781003266310
3. Yechout TR, Morris SL, Bossert DE, et al. Introduction to Aircraft Flight Mechanics. American Institute of Aeronautics and Astronautics; 2003. doi: 10.2514/4.862069
4. Etkin B, Reid LD. Dynamics of Flight: Stability and Control, 3rd ed. John Wiley & Sons; 1996.
5. Gao N, Xie C, An C, et al. Unified Aeroelastic and Flight Dynamics Formulation Based on State-Space Unsteady Aerodynamics. AIAA Journal. 2026; 64: 1–18. doi: 10.2514/1.J065498
6. Boeing Commercial Airplanes. Statistical Summary of Commercial Jet Airplane Accidents: Worldwide Operations 1959–2025. The Boeing Company; 2026.
7. Langton R. Stability and Control of Aircraft Systems: Introduction to Classical Feedback Control. John Wiley & Sons; 2006.
8. Stevens BL, Lewis FL, Johnson EN. Aircraft Control and Simulation: Dynamics, Controls Design, and Autonomous Systems, 3rd ed. John Wiley & Sons; 2015. doi: 10.1002/9781119174882
9. Liang Y, Wang R, Lei J, et al. An analysis of stability margin for altitude control of aircraft based on overload

control. In: Meng W (editor). Fourth International Symposium on Control Engineering and Robotics (ISCER 2025), Proceedings of the Fourth International Symposium on Control Engineering and Robotics; 23–25 June 2025; Shenzhen, China. SPIE; 2025. 13735. doi: 10.1117/12.3081984

10. Zhang Z, Zhou D, Wang Y, et al. Adaptive PI Control Based Stability Margin Configuration of Aircraft Control Systems with Unknown System Parameters and Time Delay. Journal of Systems Science and Complexity. 2024; 37(4): 1507–1525. doi: 10.1007/s11424-024-3364-0
11. Özer SM. Delay Effects in Stability Augmentation System of Aircraft Longitudinal Dynamics: A Case Study on Boeing 747. IEEE Access. 2025; 13: 217232–217244. doi: 10.1109/ACCESS.2025.3648550
12. Pollack T, van Kampen EJ. Robust Stability and Performance Analysis of Incremental Dynamic-Inversion-Based Flight Control Laws. Journal of Guidance, Control, and Dynamics. 2023; 46(9): 1785–1798. doi: 0.2514/1.G006576
13. Liu J. The angle of attack and side-slip angle estimation for civil aircraft. Journal of Physics: Conference Series. 2023; 2569: 012072. doi: 10.1088/1742-6596/2569/1/012072
14. Gong Z, Di W, Jiang Y, et al. Flexible calorimetric flow sensor with unprecedented sensitivity and directional resolution for multiple flight parameter detection. Nature Communications. 2024; 15: 3091. doi: 10.1038/s41467-024-47284-7
15. Karimli T, Guliyev R, Nasibova G. Modeling of a Complex Digital Air Data System for Measuring Attitude and Flight Direction of Aircraft. International Journal of Transportation Research and Technology. 2025; 2(1): 37–48. doi: 10.71108/transporttech.vm02is01.03
16. Zhang C, Pan W, Zhu Y, et al. Theoretical Assessment of Runway Capacity for Training and Transport Airport Considering Wake Vortex Encounter Safety: A Case Study of Luoyang Beijiao Airport. Applied Sciences. 2025; 15(20): 11273. doi: 10.3390/app152011273
17. Matt JJ, Chao H, Lin Z, et al. Simplified Wake Vortex Encounter Modeling and Inner Loop Control for Small UAS. In: Proceedings of the AIAA SCITECH 2023 Forum; 23–27 January 2023; National Harbor, MD, USA. doi: 10.2514/6.2023-0801
18. Figat M, Kwiek A. Analysis of longitudinal dynamic stability of tandem wing aircraft. Aircraft Engineering and Aerospace Technology. 2023; 95(9): 1411–1422. doi: 10.1108/AEAT-11-2022-0328
19. Pallett EHJ, Coyle S. Automatic Flight Control, 4th ed. Blackwell Science; 1993.
20. Liu J. Integrated design of lateral-directional control law and vertical tail load for civil aircraft. Journal of Physics: Conference Series. 2024; 2691: 012030. doi: 10.1088/1742-6596/2691/1/012030
21. Xie G, Chen L, Qu X. Directional control law functional analysis and design for civil aircraft simulator. Journal of Physics: Conference Series. 2024; 2882: 012030. doi: 10.1088/1742-6596/2882/1/012030
22. Takahashi TT, Griffin JA, Grandhi RV. A Review of High-Speed Aircraft Stability and Control Challenges. In: Proceedings of the AIAA AVIATION 2023 Forum; 12–16 June 2023; San Diego, CA, USA. doi: 10.2514/6.2023-3231
23. Takahashi TT, Griffin JA, Grandhi RV. High-Speed Aircraft Stability and Control Metrics. Aerospace. 2025; 12(1): 12. doi: 10.3390/aerospace12010012
24. Bottigliero R, Rossano V, De Stefano G. Transonic Dynamic Stability Derivative Estimation Using Computational Fluid Dynamics: Insights from a Common Research Model. Aerospace. 2025; 12(4): 304. doi: 10.3390/aerospace12040304
25. Schütte A, Hummel D. Numerical Mach Number Studies on a Multidelta Wing Configuration with Vertical Stabilizers. Journal of Aircraft. 2025; 62(5): 1–14. doi: 10.2514/1.C038163
26. Liu S, Lyu W, Zhang Q, et al. Neural-Network-Based Incremental Backstepping Sliding Mode Control for Flying-Wing Aircraft. Journal of Guidance, Control, and Dynamics. 2025; 48(3): 600–614. doi: 10.2514/1.G008215
27. Ul Islam SA, Ali SM, Bernstein DS. A Data-Driven Stability Augmentation System for an Aircraft with Unknown Transition between Open-Loop-Stable and Open-Loop-Unstable Dynamics. In: Proceedings of the AIAA SCITECH 2025 Forum; 6–10 January 2025; Orlando, FL, USA. doi: 10.2514/6.2025-2430
28. Aslam F, Ul Islam SA, Akhtar S, et al. A Data-Driven Predictive Terrain-Following Autopilot for an Aircraft Undergoing Stability-Augmentation-System Failure. In: Proceedings of the AIAA SCITECH 2025 Forum; 6–10 January 2025; Orlando, FL, USA. doi: 10.2514/6.2025-2429